

Highlights

A vibration signal model of planetary gearboxes with unequal load sharing among planets

Haoqun Ma,Zhipeng Feng

- Vibration signal model of equal load sharing among planets
- Influence of gear meshing vibration, transfer path effects and natural frequency
- Analytical expression of Fourier spectrum
- Explanation on spectral configuration arisen from different factors

A vibration signal model of planetary gearboxes with unequal load sharing among planets

Haoqun Ma^a, Zhipeng Feng^{a,*}

^aUniversity of Science and Technology Beijing, No.30, Xueyuan Road, Haidian District, Beijing.

ARTICLE INFO

Keywords:

Unequal load sharing
Planetary gearbox
Signal model
Fault diagnosis

ABSTRACT

Planetary gearboxes feature large transmission ratios within compact volumes, because they can divide the input torque load into several paths through parallel planets. Unevenly load sharing among planets lead to inefficiency and accelerating fatigue. This paper establishes a vibration signal model to describe how the uneven distribution of planet loads affects the vibration signal composition. Compared with fixed shaft bearings, planet bearings are more prone to faults due to its excessive load. We also establish a vibration signal of planet bearing faults along with the uneven distribution of planet loads. Planet bearing faults are more difficult to diagnose due to abundant modulation sidebands arising from the unequal load sharing among planets. Numerical simulation and experimental substations agrees with the proposed theoretical model.

1. Introduction

Planets split power transmitted from the input sun gear into paralleled paths so that planetary gearboxes can withstand heavy load in a compact volume. While the special structure bring about unequal load sharing among planets.

2. Signal model

1. Planetary gearboxes have different configuration with similar layouts.
2. In this paper, we only consider the case where ring gear is fixed. (refer to the paper mentioning the sun or carrier as the fixed central part)
3. The vibration sensor is mounted on the stationary ring gear.
4. The vibration mainly origins the time-varying stiffness gear meshing. When the planet gears engage with the ring gear or sun gear, the number of the involved tooth varies with the relative rotation between gears. Thus, their contact stiffness changes at the same time. If the transmission load proximately remain constant, this system is pure parametric excited. (Add a reference about instability)
5. Specially, the torque load transferred from the central components in planetary gearboxes is split into parallel paths formed by the planets. Because of the inevitable manufacturing and assembling errors of pinholes or bearings, there are usually differences in the position of pinholes and the shape of planets. The load sharing among planets is non-uniform (collect other reasons from the Sigh's paper).
6. Another common phenomenon in planetary gearboxes is the difference in meshing phases between ring-planet and sun-planet. When this situation coincides with the load sharing inequality, a complex couple mechanism of time-varying load sharing emerges, rising extra vibrations.
7. For an individual planet, the vibration signal model can be written as

2.1. Planetary gearbox structure

A typical layout of planetary gearboxes consists of three kinds of gears mounted so that the centers of planet gears revolves around the center of sun and ring gears, as shown in Fig. 2. This paper merely discusses the common cases of speed reducers where the sun gear connects with the power input shaft and the carrier works as power output, while vibration sensors are usually mounted on the surface of the stationary ring gear in diagnostic applications.

*Corresponding author

 fengzp@ustb.edu.cn (Z. Feng)

ORCID(s): 0000-0002-3403-4386 (Z. Feng)

Nomenclature

f_c	carrier rotation frequency	L_i	bearing and gear meshing load sharing ratio of the i -th planet
f_m	gear meshing frequency	r_s	sun gear pitch radius
J	inertia moment	T_s	total torque applied on input sun gear
$k(t)$	stiffness		
k_e	effective support stiffness concerning both the		

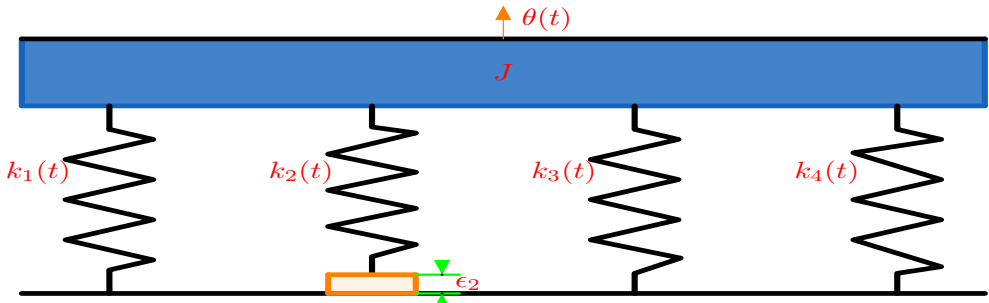


Figure 1: Vibration system of unequal load sharing among four planets.

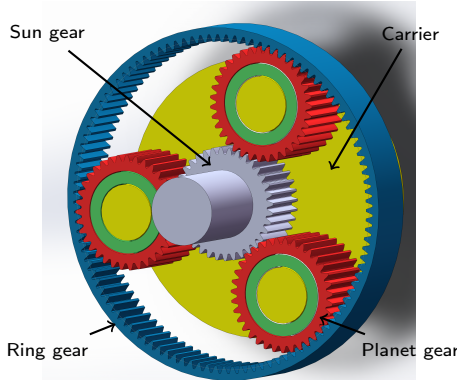


Figure 2: Configuration of planetary gearboxes.

2.2. General signal model

The vibration in planetary gearboxes mainly originates from the meshing of gears [1]. When the planet gears engage with the ring gear or sun gear, the number of the involved tooth varies with the relative rotation between gears and their contact stiffness changes consequently. The transmission load nominally remains constant and the gearbox is a parametrically excited multi-degree-of-freedom system [2].

The signal model perceived by the stationary transducer on the gearbox housing can be modelled as the summation of all planet vibration considering transfer path effects. The impulsive intensity of gear meshing is assumed to be proportional to the load applied on each planet. The vibration of each planet is divided into planet-ring and planet-sun parts. Thus, the general signal model is

$$x(t) = \sum_{i=1}^M L_i \cdot [\sigma_{ri}(t)\xi_{ri}(t) + \sigma_{si}(t)\xi_{si}(t)], \quad (1)$$

where M is the planet number, L_i denotes the load sharing coefficient, σ_{pr} and σ_{ps} denotes transfer path effect on planet-ring and planet-sun gears, respectively, ξ_{ri} and ξ_{si} are the vibration originating from the i -th planet-ring and planet-sun gears.

Nominally, all planet center distribute along circumference of the carrier evenly. Without loss of generality, the nominal angular position of first planet center is set as zero, and

$$\Theta_i = \frac{(i-1) \cdot 2\pi}{M}, \quad (2)$$

where Θ_i denotes the nominal position of i -th planet. In addition, due to the manufacturing or assembling process, each planet center deviates from the nominal position by ϵ_i . If $\epsilon_i > 0$, the planet engages with the ring or sun gear in advance, or negative error represents the engagement lag. We can assume $\epsilon_1 = 0$ in the coordinate system, because these planets locate relatively to each other. Even if $\epsilon_1 \neq 0$, we can also set $\epsilon_i = \epsilon'_i - \epsilon'_1, i \geq 2$, where ϵ'_i is i -th planet error in another coordinate system.

To reveal the spectral structure simply, the gear meshing vibration of each planet is regarded as Dirac comb function $\text{III}(t) = \sum_{i=-\infty}^{+\infty} \delta(t - i)$. The meshing frequency can be calculated by different engaging gears,

$$f_m = Z_r \cdot (f_r + f_c) = Z_p \cdot (f_p - f_c) = Z_s \cdot (f_s - f_c). \quad (3)$$

where $\{\}_r, \{\}_p, \{\}_s, \{\}_c$ denote ring gear, planet, sun gears and carrier, respectively; $Z_{\{\}}$ is the gear number and $f_{\{\}}$ is the rotating frequency.

For planet-ring gears, the planet angular position error bring about the time shift. The time shift is the angular error divided by the relatively rotating velocity. Thus, the planet-ring meshing vibration can be written as

$$\xi_{ri}(t) = A_{ri} \text{III} \left[f_m \cdot \left(t - \frac{\epsilon_i + \Theta_i}{2\pi f_c} \right) \right], \quad (4)$$

where A_{ri} is the impulsive amplitude of i -th planet-ring gear meshing, the f_m is the meshing frequency. Park et al. propose the difference between planet-ring and planet-sun meshing phase [4]. Similarly, the planet-sun meshing vibration is

$$\xi_{si}(t) = A_{si} \text{III} \left[f_m \cdot \left(t + \frac{\epsilon_i + \Theta_i}{2\pi f_s - 2\pi f_c} \right) + \frac{\varphi_i}{2\pi} \right], \quad (5)$$

where A_{si} is the impulsive amplitude of i -th planet-sun gear meshing, φ_i is the phase difference between planet-ring and planet-sun meshing for the i -th planet.

2.3. Algorithm of load sharing coefficients

The multiple paralleled power paths formed by planets can sharing torque load. This merit of planetary gearboxes will compromise when the load sharing inequality occurs. The position errors of planet pinholes or bearings in the tangential (circumferential) direction happening in manufacturing and assembling lead to the non-uniform loads on planets [5]. To partly centralize the uneven load, planetary gearboxes usually permit at least one floating central member (sun gear or carrier). The formula of load sharing ratio of a 4-planet planetary gearbox as follows [6]

$$k_e = \frac{1}{k_{rp} + k_{sp}} + \frac{1}{k_b}, \quad (6)$$

where k_{rp} and k_{sp} are the meshing stiffness of planet-ring and planet-sun, respectively, k_b is the planet bearing stiffness.

$$e_i = 2(R_p - R_s) \sin(\epsilon_i/2) \cos(\epsilon_i/2), \quad (7)$$

where R_p is the planet radius, R_s is the sun radius, ϵ_i is the angular position error the i -th planet.

Unequal load sharing will gives rise to non-uniform impulsive intensity. The acceleration are linearly affected by the dynamic force exerted. Thus, the vibration amplitude of each planet is assumed to be proportional to the load

Unequal planet load sharing

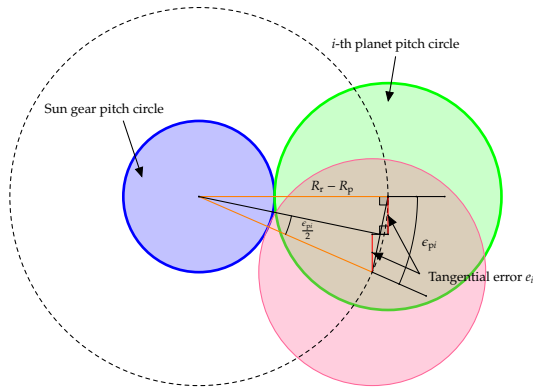


Figure 3: Tangential error calculation (correct the ϵ_{pi})

applied on it [7]. In other words, planet load modifies the amplitude of the vibration signal. Moreover, the unevenly planet distribution along the angular position of carrier also has phase modulation when the transfer path is considered simultaneously. These effects will be illustrated explicitly in the later Section 4.

2.4. Transfer paths

The vibration originating from the planet meshing with ring or sun gear propagate through several paths to the stationary sensor mounted on the case. As demonstrated in Fig. 4, there are three paths for planet-ring and planet-sun gear meshing, respectively. These transfer paths can be categorized into two types, depending on whether or not they pass through bearings. The paths passing through bearings (path 2, 3, 5, 6 in Fig. 4) must transfer via the gearbox housing to reach the sensor fixed on the top. Compared with the paths merely passing through gears (path 1, 4 in Fig. 4), these paths passing bearings are longer and more likely to be attenuated by the lubricating oil layer in bearings [8]. To simplify modelling, only the shorter paths (path 1, 4 in Fig. 4) are concerned in this paper.

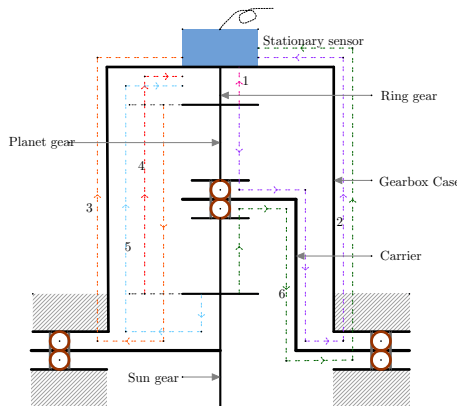


Figure 4: Transfer paths of gear meshing vibration.add explanation on path number. from where to where.

The lengths of path 1 and path 4 vary with the circumferential position of carrier. For each planet, the meshing vibration points get close to the fixed sensor as the planet approaches the top surface of gearbox case. When the planet reaches the climax of its revolution circle, the fixed transducer perceives the maximum impulsive strength. While the planet arrives at the case bottom, the perceived impulses are most weakened. The path 1 length is triangle wave of time

(as shown in Fig. 5) when planetary gearboxes operate at a constant speed and planet distributes evenly,

$$l_{ri}(t) = \begin{cases} 2\pi R_r f_c \left| t - \left(\frac{\epsilon_i + \Theta_i}{2\pi f_c} + \frac{n}{f_c} \right) \right|, & \frac{n}{f_c} - \frac{1}{2Mf_c} + \frac{\epsilon_i + \Theta_i}{2\pi f_c} \leq t < \frac{n}{f_c} + \frac{1}{2Mf_c} + \frac{\epsilon_i + \Theta_i}{2\pi f_c}, n \in \mathbb{Z}, i = 1, 2, \dots, M \\ +\infty, & \text{otherwise} \end{cases}, \quad (8)$$

where M is the planet number. The path 4 is the sum of the diameter of the planet pitch circle and l_{ri} ,

$$l_{si}(t) = l_{ri} + 2R_p. \quad (9)$$

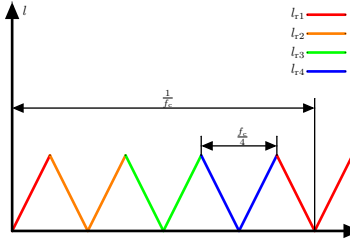


Figure 5: Transfer Path 1 length function of time. vary the line type for different legends. Add the transfer effect function of time

This attenuation effect with regard to the path length can be characterized as window functions such as Hanning window or Gaussian window [9]. In this paper, we apply the Gaussian window describing the time-varying transfer path effect,

$$\sigma(l) = F \exp\left(-\frac{l}{a}\right), \quad (10)$$

where l is the length of a transfer path, F represents for the strength factor and a is the attenuation factor. F is proportional to the input torque T_s , here we assume $F = T_s/300$. The larger a is, the longer impulses can propagate without a large energy loss. Given Eq. (9) and Eq. (10), we can deduce the proportional relationship between path 1 and path 4,

$$\sigma(l_{si}) = F \exp\left(-\frac{l_{ri} + 2R_p}{a}\right) = \exp\left(-\frac{2R_p}{a}\right) \cdot \sigma(l_{ri}). \quad (11)$$

For simplicity, we set the $\sigma_i(t) = \sigma[l_{ri}(t)]$ and $\eta = \exp(-\frac{2R_p}{a})$. Fig. 5 shows that $\sigma_i(t)$ shifts in time by $(\epsilon_i - \Theta_i)/(2\pi f_c)$ relative to σ_1 :

$$\sigma_i(t) = \sigma_1\left(t - \frac{\epsilon_i + \Theta_i}{2\pi f_c}\right). \quad (12)$$

Because the transfer path effect function is the exponential function shifting along the time axis with a fixed interval, it can be rewritten as the convolution of exponential function and Dirac comb function with the carrier rotation period $1/f_c$.

$$\sigma_i(t) = \sigma_0(t) * \text{III}\left[f_c\left(t - \frac{\epsilon_i + \Theta_i}{2\pi f_c}\right)\right], \quad (13)$$

where

$$\sigma_0(t) = \begin{cases} F \exp\left(\frac{-2\pi R_f f_c |t|}{a}\right), & \frac{-1}{2Mf_c} \leq t < \frac{1}{2Mf_c} \\ 0, & \text{otherwise.} \end{cases} \quad (14)$$

2.5. Natural frequency

In the above discussion, the gear meshing vibration is simply considered as Dirac impulses. In practice, every impact arising from different components will excite the machine natural frequency. The excited resonance affects the spectral structure globally: the amplitudes of the vibration frequencies around the natural frequency are reinforced and other amplitudes are attenuated. The resonance features a harmonic wave with the amplitude attenuating exponentially, like the vibration of a spring-mass-damper,

$$\lambda(t) = \begin{cases} \exp(-t/\beta) \cdot \sin(2\pi f_n t), & t \geq 0 \\ 0, & t < 0 \end{cases}, \quad (15)$$

where $\beta > 0$ is the structural damping coefficient, f_n is the natural frequency.

Every time a gear meshing vibration occurs, the machine's natural vibration is excited. This process is mathematically equivalent to the convolution of the impact function of the meshing vibration with the exponentially attenuated harmonic function of the natural vibration. Therefore, considering the effect of the natural vibration, the above signal model can be updated into

$$\tilde{x}(t) = \lambda(t) * \sum_{i=1}^M L_i \sigma_i(t) \left\{ \text{III} \left[f_m \cdot \left(t - \frac{\epsilon_i + \Theta_i}{2\pi f_c} \right) \right] + \eta \text{III} \left[f_m \cdot \left(t + \frac{\epsilon_i + \Theta_i}{2\pi f_s - 2\pi f_c} \right) + \frac{\varphi_i}{2\pi} \right] \right\}, \quad (16)$$

where $*$ denotes convolution.

For machines with the same configuration, when the load distribution of the planet is uneven, the contact stiffness of the transfer path of each planet inside the planetary gearbox will decrease relative to the case of the uniform load distribution. As a result, The decrease of internal contact stiffness will lead to the decrease of natural frequency of the whole system. Therefore, the variation of the system's natural frequency can be used as a circumstantial evidence to diagnose the load distribution among planets.

If the planet pinhole distribute evenly on the carrier, the number of the planets bearing the input load varies as the applied load increases gradually. When the load starts at almost zero, only three planets or one pair of diagonal planets simultaneously engaging with sun and ring gear [6]. In this circumstance, load sharing coefficients $L_i = 0$ for the unloaded planets. With the ascending input load, another pair of gears get involved. At the same time, the entire transmission system stiffen because more gears support the connection between the input and output. The natural frequency rises along with the system stiffness because the natural frequency equals the square root of stiffness over mass.

3. Spectral structure

In this section, we will derive the spectral structure of the above proposed signal model for the in-depth understanding of planetary gearbox vibration. Because natural vibration merely affects the spectral envelope shape, we can consider it separately later on. The gear meshing vibration (Eq. (4) and Eq. (5)) and transfer path effect arising from the carrier rotation $\sigma_i(t)$ are periodic with periods $1/f_m$ and $1/f_c$, respectively. According to Eq. (3) and $f_r = 0$, $f_m = Z_r \cdot f_c$.

Apply Fourier transform to the planet-ring vibration, yields

$$\begin{aligned}
\mathcal{F} [\sigma_{ri}(t)\xi_{ri}(t)] &= \mathcal{F} \left\{ \sigma_0(t) * \text{III} \left[f_c \cdot (t - \frac{\epsilon_i + \Theta_i}{2\pi f_c}) \right] \cdot A_{ri} \text{III} \left[f_m \cdot (t - \frac{\epsilon_i + \Theta_i}{2\pi f_c}) \right] \right\} \\
&= A_{ri} \cdot \mathcal{F} [\sigma_0(t)] \cdot \mathcal{F} \left\{ \text{III} \left[f_c \cdot (t - \frac{\epsilon_i + \Theta_i}{2\pi f_c}) \right] \right\} * \mathcal{F} \left\{ \text{III} \left[f_m \cdot (t - \frac{\epsilon_i + \Theta_i}{2\pi f_c}) \right] \right\} \\
&= A_{ri} \cdot \hat{\sigma}_0(f) \cdot \frac{\text{III} \left(\frac{f}{f_c} \right) \exp \left[-\frac{jf(\epsilon_i + \Theta_i)}{f_c} \right]}{\sqrt{2\pi} f_c} * \frac{\text{III} \left(\frac{f}{Z_r f_c} \right) \exp \left[-\frac{jf(\epsilon_i + \Theta_i)}{f_c} \right]}{\sqrt{2\pi} Z_r f_c} \\
&= A_{ri} \cdot \frac{\hat{\sigma}_0(f)}{2\pi Z_r f_c^2} \cdot \sum_{m=-\infty}^{+\infty} \sum_{n=-\infty}^{+\infty} \delta [f - (mZ_r + n)f_c] \exp [-j(mZ_r + n)(\epsilon_i + \Theta_i)] . \tag{17}
\end{aligned}$$

where $\mathcal{F}\{\cdot\}$ denotes Fourier transform, $\hat{\sigma}_0(f)$ is the Fourier spectrum of $\sigma_0(t)$, $\delta\{\cdot\}$ denotes Dirac impulse, $*$ denotes convolve. The convolution between two Dirac comb functions equals the summation of all shifted Dirac impulses. Similarly, the i -th planet-sun gear vibration is:

$$\begin{aligned}
\mathcal{F} [\sigma_{si}(t)\xi_{si}(t)] &= \mathcal{F} \left\{ \eta \cdot \sigma_0(t) * \text{III} \left[f_c \cdot (t - \frac{\epsilon_i + \Theta_i}{2\pi f_c}) \right] \cdot A_{si} \text{III} \left[f_m \cdot (t + \frac{\epsilon_i + \Theta_i}{2\pi f_s - 2\pi f_c}) + \frac{\varphi_i}{2\pi} \right] \right\} \\
&= \eta \cdot A_{si} \cdot \mathcal{F} [\sigma_0(t)] \cdot \mathcal{F} \left\{ \text{III} \left[f_c \cdot (t - \frac{\epsilon_i + \Theta_i}{2\pi f_c}) \right] \right\} * \mathcal{F} \left\{ \text{III} \left[f_m \cdot (t + \frac{\epsilon_i + \Theta_i}{2\pi f_s - 2\pi f_c}) + \frac{\varphi_i}{2\pi} \right] \right\} \\
&= \eta \cdot A_{si} \cdot \hat{\sigma}_0(f) \cdot \frac{\text{III} \left(\frac{f}{f_c} \right) \exp \left[-\frac{jf(\epsilon_i + \Theta_i)}{f_c} \right]}{\sqrt{2\pi} f_c} * \frac{\text{III} \left(\frac{f}{Z_r f_c} \right) \exp \left[\frac{jf(\epsilon_i + \Theta_i)}{f_c - f_s} \right] \exp \left(\frac{\varphi_i f}{2\pi Z_r f_c} \right)}{\sqrt{2\pi} Z_r f_c} \\
&= \eta \cdot A_{si} \cdot \frac{\hat{\sigma}_0(f)}{2\pi Z_r f_c^2} \cdot \sum_{m=-\infty}^{+\infty} \sum_{n=-\infty}^{+\infty} \delta [f - (mZ_r + n)f_c] \exp [j(Z_s m - n)(\epsilon_i + \Theta_i)] \exp(jm\varphi_i), \tag{18}
\end{aligned}$$

where $Z_s(f_c - f_s) = Z_r f_c = f_m$ is applied. Combine the above planet-ring and planet-sun vibration for all planets:

$$\begin{aligned}
X(f) &= \sum_{i=1}^M L_i \cdot \{ \mathcal{F} [\sigma_{ri}(t)\xi_{ri}(t)] + \mathcal{F} [\sigma_{si}(t)\xi_{si}(t)] \} \\
&= \sum_{i=1}^M L_i \cdot \left\{ A_{ri} \cdot \frac{\hat{\sigma}_0(f)}{2\pi Z_r f_c^2} \cdot \sum_{m=-\infty}^{+\infty} \sum_{n=-\infty}^{+\infty} \delta [f - (mZ_r + n)f_c] \exp [-j(mZ_r + n)(\epsilon_i + \Theta_i)] \right. \\
&\quad \left. + \eta \cdot A_{si} \cdot \frac{\hat{\sigma}_0(f)}{2\pi Z_r f_c^2} \cdot \sum_{m=-\infty}^{+\infty} \sum_{n=-\infty}^{+\infty} \delta [f - (mZ_r + n)f_c] \exp [j(Z_s m - n)(\epsilon_i + \Theta_i)] \exp(jm\varphi_i) \right\} \\
&= \frac{\hat{\sigma}_0(f)}{2\pi Z_r f_c^2} \sum_{m=-\infty}^{+\infty} \sum_{n=-\infty}^{+\infty} \delta [f - (mZ_r + n)f_c] \left\{ \sum_{i=1}^M L_i \cdot A_{ri} \cdot \exp [-j(mZ_r + n)(\epsilon_i + \Theta_i)] \right. \\
&\quad \left. + \eta \cdot L_i \cdot A_{si} \cdot \exp(jm\varphi_i) \cdot \exp [j(mZ_r - n)(\epsilon_i + \Theta_i)] \right\}. \tag{19}
\end{aligned}$$

We assume the isotropy of planet and the amplitudes of i -th planet gear meshing impacts A_{ri} and A_{si} remain the same for every planet, that is $A_{ri} = A_{r1}$, $A_{si} = A_{s1}$. When all planets locate at the nominal positions ($\epsilon_i = 0$), each

planet bears the same torque ($L_i = L_1$), The $X(f)$ in the ‘perfect’ case is

$$X(f) = \frac{L_1 \cdot \hat{\sigma}_0(f)}{2\pi Z_r f_c^2} \sum_{m=-\infty}^{+\infty} \sum_{n=-\infty}^{+\infty} \delta [f - (mZ_r + n)f_c] \left\{ \sum_{i=1}^M A_{ri} \exp [-j(mZ_r + n)\Theta_i] + \eta A_{si} \exp (jm\varphi_i) \exp [j(mZ_r - n)\Theta_i] \right\}, \quad (20)$$

where

$$\sum_{i=1}^M \exp [-j(mZ_r + n)\Theta_i] = \sum_{i=1}^M \exp [-j(mZ_r + n) \frac{2\pi(i-1)}{M}] = \begin{cases} M, & \frac{mZ_r+n}{M} \in \mathbb{N} \\ 0, & \frac{mZ_r+n}{M} \notin \mathbb{N} \end{cases}, \quad (21)$$

$$\sum_{i=1}^M \exp [j(mZ_s - n)\Theta_i] = \sum_{i=1}^M \exp [j(mZ_s - n) \frac{2\pi(i-1)}{M}] = \begin{cases} M, & \frac{mZ_s-n}{M} \in \mathbb{N} \\ 0, & \frac{mZ_s-n}{M} \notin \mathbb{N} \end{cases}. \quad (22)$$

According to the above Eq. (21) and Eq. (22), when $(mZ_s - n)$ or $(mZ_s - n)$ is the multiple of planet number M , the corresponding Fourier coefficient is nonzero. The carrier harmonics only peak at the multiple of planet number M when planet distributes evenly. Interestingly, all planet distributes evenly ($\epsilon_i = 0$) can only be achieved when the condition $(Z_r + Z_s)/M \in \mathbb{N}$ is guaranteed (explanations see Appendix). Therefore, $(mZ_r + n)/M$ and $(mZ_s - n)/M$ will be integers at one time.

When $\epsilon_i \neq 0$, all carrier harmonic $(mZ_r + n)$ and $(mZ_s - n)$ will appear with their amplitude arising from planet-ring meshing ($\sum_{i=1}^M L_i \exp [-j(mZ_r + n)(\epsilon_i + \Theta_i)]$) and planet-sun meshing ($\sum_{i=1}^M L_i \exp [-j(mZ_s - n)(\epsilon_i + \Theta_i)]$), respectively. For example, the second planet carries all load (the $L_2 = 1$ and $L_i = 0, i \neq 2$), the $(mZ_r + n)$ order harmonic manifests itself with the amplitude of $\sum_{i=1}^M L_i \exp [-j(mZ_r + n)(\epsilon_i + \Theta_i)]$, which is nonzero. The amplitudes of the planet number multiples of carrier harmonics scale down to $\exp [j(mZ_r + n)\epsilon_i]$ and $\exp [j(mZ_s - n)\epsilon_i]$, respectively.

Natural vibration further scales the amplitude of spectral components. Apply the convolution theorem to the signal model considering natural vibration (Eq. (16)), the final version of spectrum:

$$\tilde{X}(f) = \mathcal{F} [\lambda(t) * x(t)] = \mathcal{F} [\lambda(t)] \cdot \mathcal{F} [x(t)] = \hat{\lambda}(f) \cdot \tilde{X}(f) \quad (23)$$

where $\hat{\lambda}(f)$ is the Fourier transform of $\lambda(t)$:

$$\hat{\lambda}(f) = \frac{\sqrt{2\pi}\beta^2 f_n}{-4\pi^2\beta^2 f^2 + 4\pi^2\beta^2 f_n^2 + 1 - j4\pi\beta f} \quad (24)$$

4. Discussion on model factors

We use MATLAB[®] to simulate the proposed signal model. To validate the generality of the propose model, we take different planet pinhole position errors, planet numbers and input torques into account. The simulation parameters are listed in Table ??.

In general, if the planet locates the nominal position, only the planet number multiples of carrier harmonics appear (give more specific results in figures), which accords with the Eq. (21) and Eq. (22). When the planet center deviates from the nominal position, other carrier orders emerges. Differing from the conclusion in [9], the dominant planet number multiple peaks do not shrink too, because we also consider the phase modulation induced by the pinhole position errors.

Fig. ?? and Fig. 6 explain the mechanism of shifted natural frequency – the resonance frequency shift from 300Hz to 400Hz. With the limited measurement conditions about natural frequency in industrial applications, the above natural frequency shift can only be validated qualitatively. The signal model in Eq. (16) indicates the natural frequency affects the spectral envelope shape. As the load increases, the envelope peak shifting to a higher frequency signifies the unequal load sharing among planets.

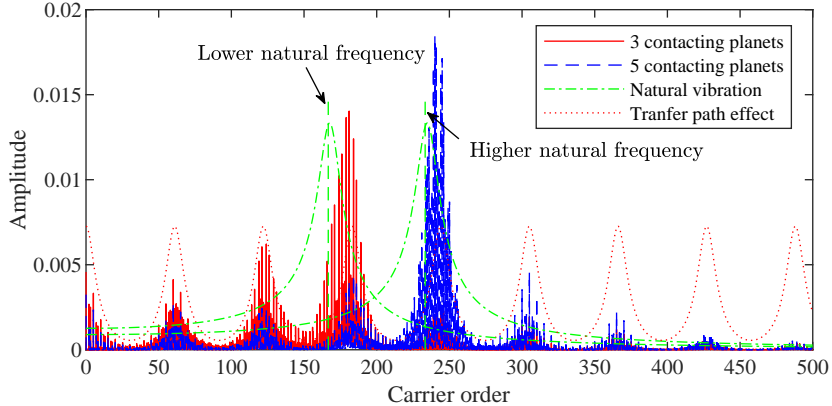


Figure 6: Spectral summit cluster shifts towards a lower frequency due to the uneven load distribution of planets

The extra sidebands at non M multiples of carrier orders can be attributed by the phase modulation effects (with a period of carrier rotation period and fluctuates at each planet position (both time and space)).

The amplitude envelope sharpe can also evidence the existence of planet position shifts. Because the support stiffness weakens, the resonance frequency of the entire system shift towards the y-axis. Fig. ?? and Fig. 6 show the resonance frequency shift from 300Hz to 400Hz.

4.1. Different planet numbers

When at least one central members can float along the radial direction, three planets can offset the influence of uneven load distribution arising from limited pinhole position errors. The condition of floating central members can be satisfied commonly, because the manufacturers deliberately design separable sun gears and flexible couplings. When tangential error in planet pinhole occur, the time shifts to the transfer path effects still make the impulsive intervals between adjacent planets uniform. Fig 7(b) present the quasi phase modulation – if we regard all planets as one – in time domain. The corresponding spectrum also manifests the non planet number ($M = 3$) peaks. In the baseline case where these pinhole errors are absent, the carrier orders merely appear at the multiples of three.

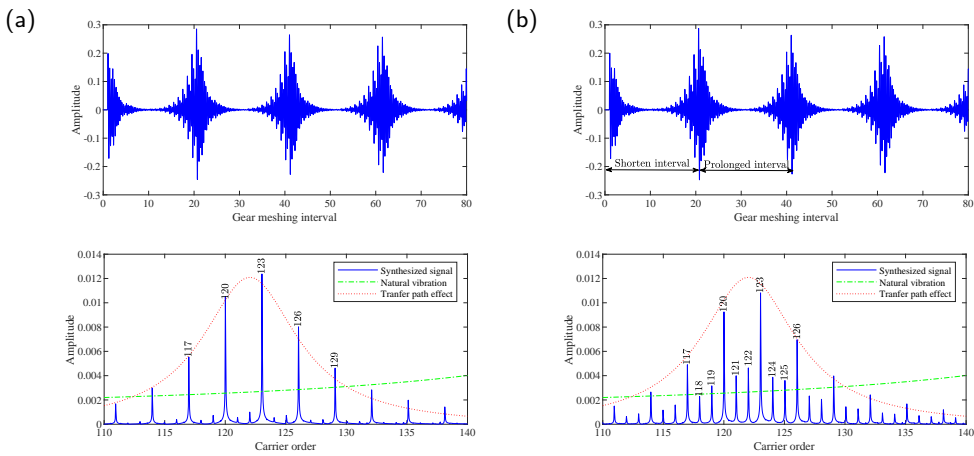


Figure 7: Simulated signals of planetary boxes of 3 planets: (a) normal case; (b) 0.5° position error on second planet pinhole.

In cases where planet number $M \geq 4$, floating members in planetary gearboxes cannot neutralize all effects on load sharing conditions caused by planet pinhole position errors. The time domain signals in Fig. 8(b) ($M = 4$) demonstrates

the pinhole errors modulates the timing and strength of each planet impulse at the same time. Shown in the Fourier spectra of fault cases, the quasi amplitude and frequency modulation gives rise to the extra sidebands emerge at the non M multiples. While carrier orders only peak with the intervals of planet number in Fig. 8(a) ($M = 4$).

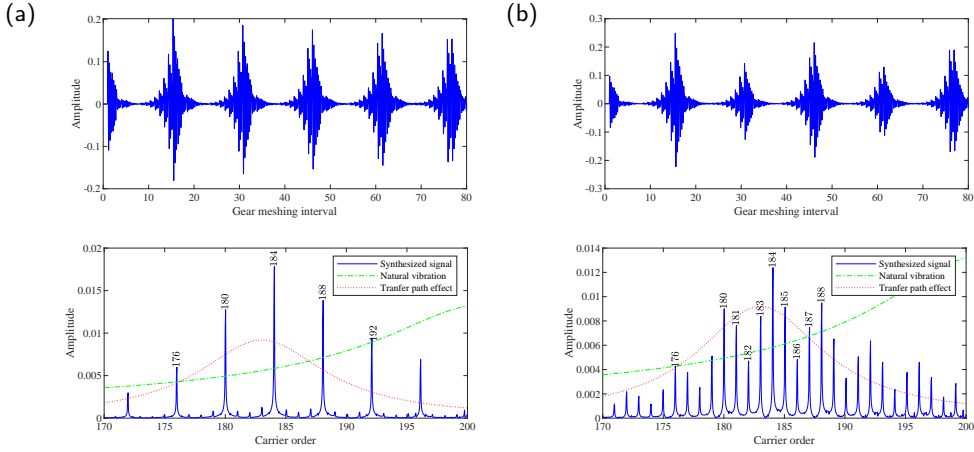


Figure 8: Simulated signals of planetary boxes of 4 planets: (a) normal case; (b) 0.5° position error on second planet pinhole.

4.2. Effects of input torque

As explained in the Section 2.4, the input torque affects the impulsive strengths of planets contacting with sun and ring gears, so as to scale the whole signal amplitudes. Fig. 9 shows that the larger input torque is applied, the higher signal amplitude in both time and frequency domains.

The input torque also affects the numbers of contacting planets. As the input torque increases from a lower value, more planets get involved in bearing load gradually. Thus, the natural frequency of the system rises. Fig. 10 presents the natural frequency shifts in spectrum. In addition, the larger input torque can improve load sharing conditions to be more uniform. Extra non M multiples shrinks relatively to the dominant M multiples.

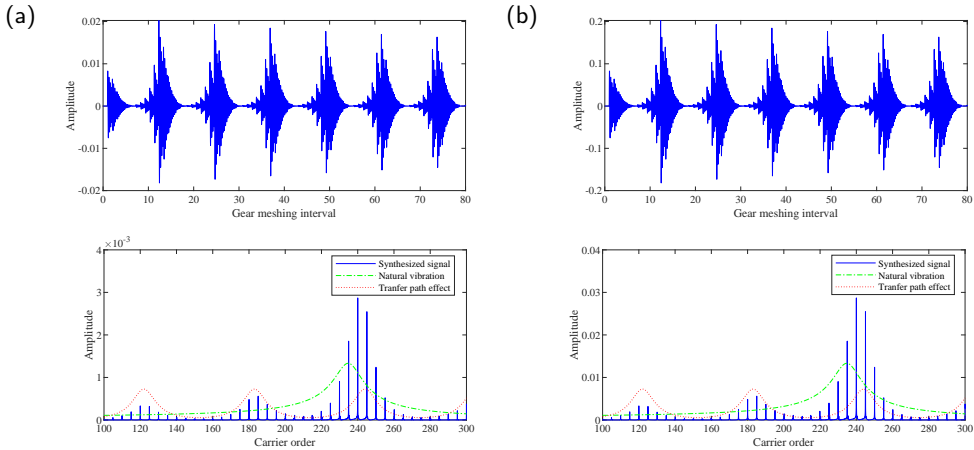


Figure 9: Simulated signals of normal planetary boxes with different input torques: (a) $T_s = 30 \text{ N m}$; (b) $T_s = 300 \text{ N m}$.

4.3. Severity levels of pinhole error

The severity of pinhole error mainly influences the signal spectra in two stages. At the beginning the planetary gearbox is free of pinhole errors. All planets bear the load evenly with the same strength as shown in time domain of

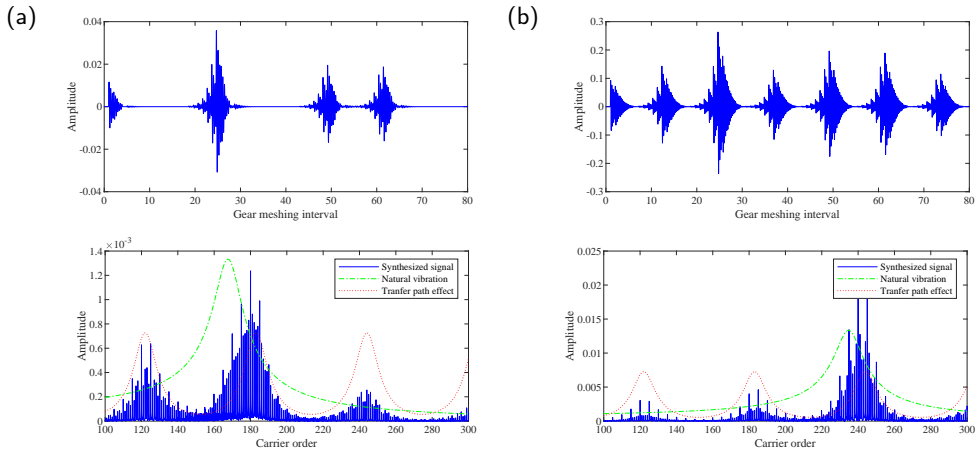


Figure 10: Simulated signals of faulty planetary boxes with 0.4° error in the third planet pinhole and different input torques: (a) $T_s = 30 \text{ N m}$; (b) $T_s = 300 \text{ N m}$.

Fig. ??(a), and peaks only exist at the multiples of planet number ($M = 6$). When a slight error (0.1° on the fourth planet pinhole) occurs, Fig. 11(b) demonstrates the non M multiples of carrier orders emerge in spectrum. At the first stage, an increasing error level (1°) leads to the amplified the components of non M multiples clustering around the dominant peaks, as presented in Fig. ??(c). At the second stage, if we continually enlarges the error to 2.1° , a pair of planets will separate from contact and the location of envelope summit along with the system natural frequency will decrease to a lower range. Fig. 11(d) illustrates this phenomenon.

5. Experimental validation

We implemented experiments to substantiate the proposed signal model and the above theoretical derivation.

5.1. Experimental settings

We set up a test rig consisting of a motor, a planetary gearbox, an encoder, a torque transducer and a generator as load, as shown in Fig. ???. Besides a normal planetary gearbox with four planets as baseline, we designed a fault case where one planet pinhole ahead of the nominal position by 0.1° , demonstrated in Fig. 13. The gearbox's configuration parameters are listed in Table ???. The rotating frequency of sun gear is 2.2 Hz. 30 N m load is applied. The gear meshing frequency is f_m and carrier frequency is f_c .

5.2. Experimental data analysis

Fig. 14 overviews the spectra of normal and fault cases. Generally, the natural vibration and transfer path effects jointly shape the envelopes of the normal and fault spectra. By contrast, the envelope summit of normal spectrum locates at the higher frequency range than the fault case since the natural frequency of normal case is higher. This indicates that the pinhole position error can cause planets to disconnect with sun or ring gears, verifying the natural frequency shift described in Section 2.5.

The signal of unequal load sharing displays more irregular impulses within one carrier rotation period, demonstrated in Fig. 15(b). While the impulsive amplitudes and intervals are more evenly distributed in the normal case (Fig. ??(a)). By comparison between frequency domains, non M multiples of carrier order peaks clearly in the fault case, evidencing the non-uniform load distribution among planets. The unobtrusive noise components are attributed to the inevitable errors during manufacturing and assembling. Conclusion

Appendix

As shown in Fig. 16. The pitch circle of planet gear rolls along the pitch circle of sun gear. When sun gear and ring gear are both fixed, the planet can only assembled at finite discrete angular positions. The minimum angular between

Unequal planet load sharing

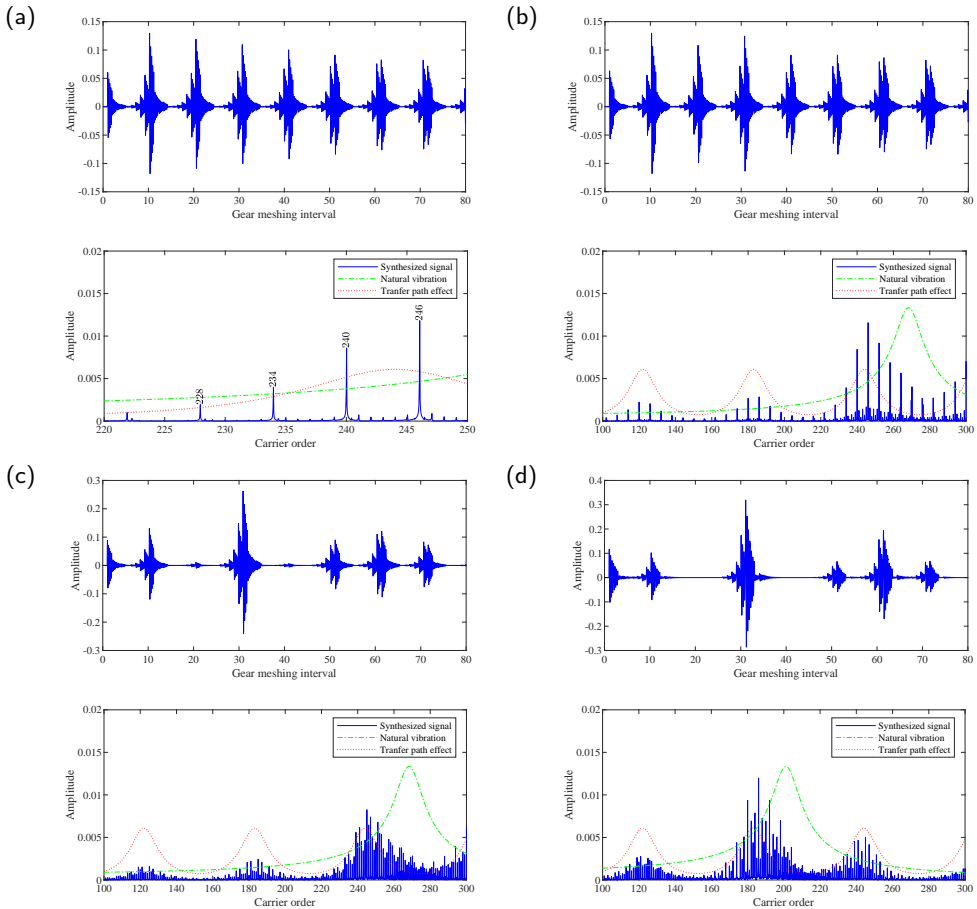


Figure 11: Simulated signals of planetary boxes with errors on the fourth planet in various severity levels: (a) normal; (b) 0.1°; (c) 1°; (d) 2.1°.

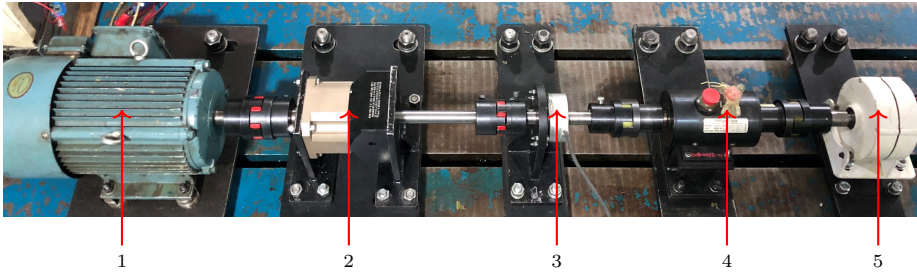


Figure 12: Planetary gearbox test rig: 1. induction motor; 2. planetary gearbox; 3. rotary encoder; 4. torque transducer and 5. generator.

two adjacent positions can be calculated as follows. Imagine the sun gear ‘rotates’ an entire tooth, and a planet rotates a distance along with the pinhole circle on the carrier. The transmission ratio between carrier and sun gear is

$$\text{Transmission ratio} = \frac{Z_s}{Z_s + Z_r} \quad (25)$$



Figure 13: Planetary gearbox with a pinhole position error

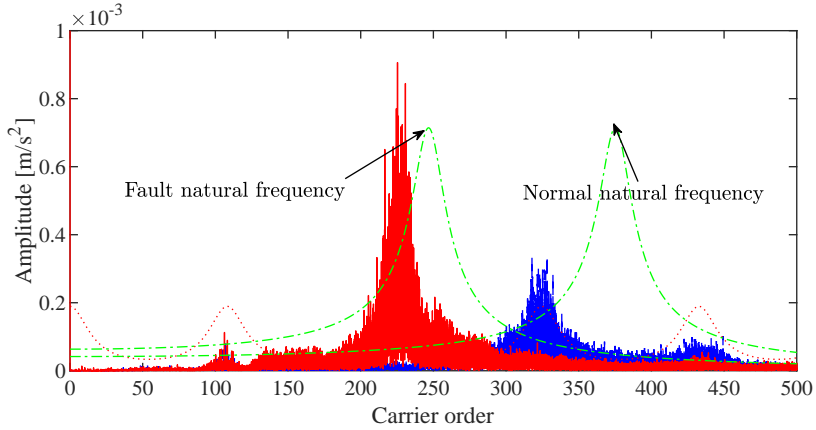


Figure 14: Spectrum overview of experimental data

the angle the sun gear rotates is: $\frac{P}{R_s}$, where P is the tooth spacing (base pitch). So the distance the pinhole center rotates is

$$(R_s + R_p) \cdot \frac{P}{R_s} \cdot \frac{Z_s}{Z_s + Z_r} = \frac{R_s + R_p}{R_s + R_r} \cdot P = \frac{R_s + R_p}{R_s + R_s + 2R_p} \cdot P = \frac{P}{2} \quad (26)$$

Thus, the angle the planet-carrier rotates is

$$\lambda = \frac{P}{2} \cdot \frac{1}{R_p + R_s} = \frac{P}{R_r + R_s} \quad (27)$$

According to the definition of module of gear $m = \frac{D}{Z} = \frac{P}{\pi}$, the Eq. (27) can be rewritten as:

$$\lambda = \frac{P \cdot 2}{D_r + D_s} = \frac{2\pi m}{m \cdot (Z_r + Z_s)} = \frac{2\pi}{Z_r + Z_s}, \quad (28)$$

The planets can only locate finite angular positions with minimum space . When planets locate uniformly at angular positions $\frac{2\pi(i-1)}{M}$, the $Z_r + Z_s$ must be an integer multiple of planet number M .

References

- [1] P. Velex, L. Flamand, Dynamic response of planetary trains to mesh parametric excitations, Journal of mechanical design 118 (1) (1996) 7–14.

Unequal planet load sharing

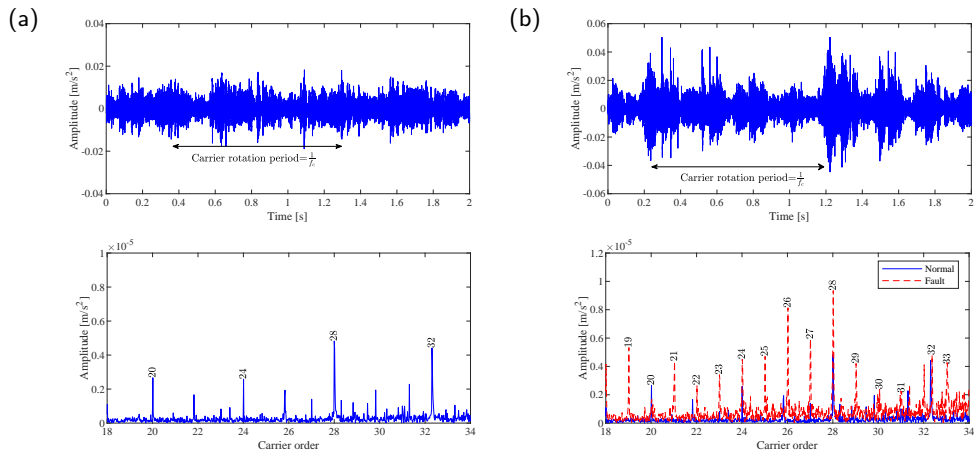


Figure 15: Experimental data analysis in time and frequency domains: (a) normal case; (b) fault case.

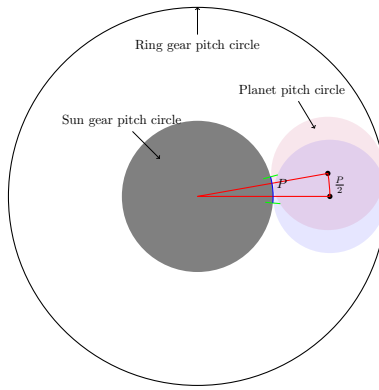


Figure 16: The minimum angle between two adjacent planet possible positions

- [2] G. D. Acar, B. F. Feeny, Approximate floquet analysis of parametrically excited multi-degree-of-freedom systems with application to wind turbines, *Journal of vibration and acoustics* 141 (1).
- [3] F. M. Arscott, *Periodic differential equations: an introduction to Mathieu, Lamé, and allied functions*, Vol. 66, Elsevier, 2014.
- [4] R. G. Parker, J. Lin, Mesh phasing relationships in planetary and epicyclic gears, *Journal of Mechanical Design* 126 (2) (2004) 365–370.
- [5] A. Singh, Load sharing behavior in epicyclic gears: physical explanation and generalized formulation, *Mechanism and machine theory* 45 (3) (2010) 511–530.
- [6] H. Ligata, A. Kahraman, A. Singh, A closed-form planet load sharing formulation for planetary gear sets using a translational analogy, *Journal of mechanical design* 131 (2).
- [7] M. Inalpolat, A. Kahraman, A theoretical and experimental investigation of modulation sidebands of planetary gear sets, *Journal of Sound and Vibration* 323 (3) (2009) 677–696.
- [8] Z. P. Feng, M. J. Zuo, Vibration signal models for fault diagnosis of planetary gearboxes, *Journal of Sound and Vibration* 331 (22) (2012) 4919–4939.
- [9] W. D. Mark, J. A. Hines, Stationary transducer response to planetary-gear vibration excitation with non-uniform planet loading, *Mechanical Systems and Signal Processing* 23 (4) (2009) 1366–1381.